

Electrochemical Degradation Mechanism and Thermal Behaviors of the Stored $\text{LiNi}_{0.5}\text{Co}_{0.2}\text{Mn}_{0.3}\text{O}_2$ Cathode Materials

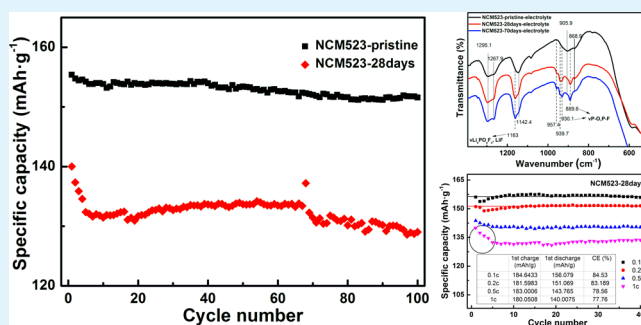
Zhiqiang Chen, Chaoyue Liu, Guiyan Sun, Xiangbang Kong, Shaobo Lai, Jiyang Li, Rong Zhou, Jing Wang,* and Jinbao Zhao*

Department of Chemistry, State Key Laboratory of Physical Chemistry of Solid Surfaces, Collaborative Innovation Center of Chemistry for Energy Materials, College of Chemistry and Chemical Engineering, Xiamen University, Xiamen 361005, China

Supporting Information

ABSTRACT: The degradation mechanism of the stored $\text{LiNi}_{0.5}\text{Co}_{0.2}\text{Mn}_{0.3}\text{O}_2$ (NCM523) electrode has been systematically investigated by combining physical and electrochemical tests. After stored at 55 °C and 80% relative humidity for 4 weeks, the NCM523 materials are coated with a layer of impurities containing adsorbed species, Li_2CO_3 and LiOH , resulting in both the weight gains of the materials and the electrochemical performance deterioration of the electrode. The impurities generated in air will react with the electrolyte and instantly turn into $\text{Li}_x\text{PO}_y\text{F}_z$ and other species containing the decomposition products of electrolyte when the stored NCM523 materials are soaked into the electrolyte, causing the charge potential plateau and the impedance to ascend. For the stored NCM523 electrodes, the huge and changeable impedance deteriorates the discharge capacity in the first 10 cycles and the discharge capacity will slowly recover and stabilize within 10 cycles when charging/discharging in 0.1 or 0.2 C. The thermal stability of the stored NCM523 materials get slightly better due to the relatively lower delithiated state after charged to 4.3 V.

KEYWORDS: $\text{LiNi}_{0.5}\text{Co}_{0.2}\text{Mn}_{0.3}\text{O}_2$, storage deterioration, thermal behaviors, cathodes, lithium-ion batteries



1. INTRODUCTION

Recently, $\text{LiNi}_x\text{Co}_y\text{Mn}_{1-x-y}\text{O}_2$ (NCM) has attracted more and more attention due to its high energy density, high power density, and relatively low cost compared to the traditional LiCoO_2 cathode materials.^{1–3} However, the NCM cathodes with Ni content greater than 60% have still faced poor thermal performance, poor cycle life, and low stability in air storage.² Until now, many research groups have dedicated to study the storage performance of NCM cathodes with high Ni content more than 60% and given a relatively detailed description of the deterioration process both in the material structure and in the electrochemical performance.^{4–9} Liu et al.⁴ believed that the surface of $\text{LiNi}_{0.8}\text{Co}_{0.2}\text{O}_2$ cathode material was covered with two thin layers, a layer of NiO-like species and a top layer consisting of adsorbed hydroxyl, bicarbonate, carbonate, and crystalline Li_2CO_3 after stored in air. Zhuang and his co-workers⁶ attributed the power and capacity loss of the $\text{LiNi}_{0.85}\text{Co}_{0.10}\text{Al}_{0.05}\text{O}_2$ cathode to the isolation of active particles by the main surface impurity Li_2CO_3 after 2 year storage, which was believed to be a low electronic and ionic conductor. Grenier et al.¹⁰ suggested that the bimodal distribution of Li at different secondary particles of $\text{LiNi}_{0.8}\text{Co}_{0.15}\text{Al}_{0.05}\text{O}_2$ (NCA) is induced by a nonuniform covering of Li_2CO_3 after exposure to the atmospheric conditions, which plays an important role in deterioration of the electrochemical performance, i.e., heightened charging

plateau, decreased capacity, etc., due to the hindering of the ion and electron pathway. Lebens-Higgins et al.¹¹ found that the contaminated NCA electrodes will be engaged with the breakdown of Li_2CO_3 in the first charging process, which will be finished at 4.25 V until the total disappear in the X-ray photoelectron spectroscopy measurement. All these references tend to relate to the downside of the performance of stored/contaminated NCM/NCA electrode to the negative effect of Li_2CO_3 . However, Li_2CO_3 serves as one of the essential inorganic parts in the total solid electrolyte interface (SEI) for anode materials, not only keeping an electron pathway among active materials, but also protecting the anode materials from self-exfoliating and being attacked by the electrolyte. It has been previously reported that Li diffusion carriers in Li_2CO_3 on cathode are Li^+ vacancies via a hopping mechanism, which are different from the diffusion carriers in the anode materials, and the conductivity in Li_2CO_3 on cathode is around 5 orders of magnitude lower than in graphite.¹² All too often, Li_2CO_3 is predicted to be decomposed at the range of 4.36–4.61 V and LiOH is in the range of 4.67–5.02 V.¹³ Also, Bi et al.¹⁴ concluded that pure Li_2CO_3 does not oxidize until 5.3 V (vs Li/Li^+) at linear sweep voltammetry and will slowly turn into

Received: May 13, 2018

Accepted: July 2, 2018

Published: July 2, 2018

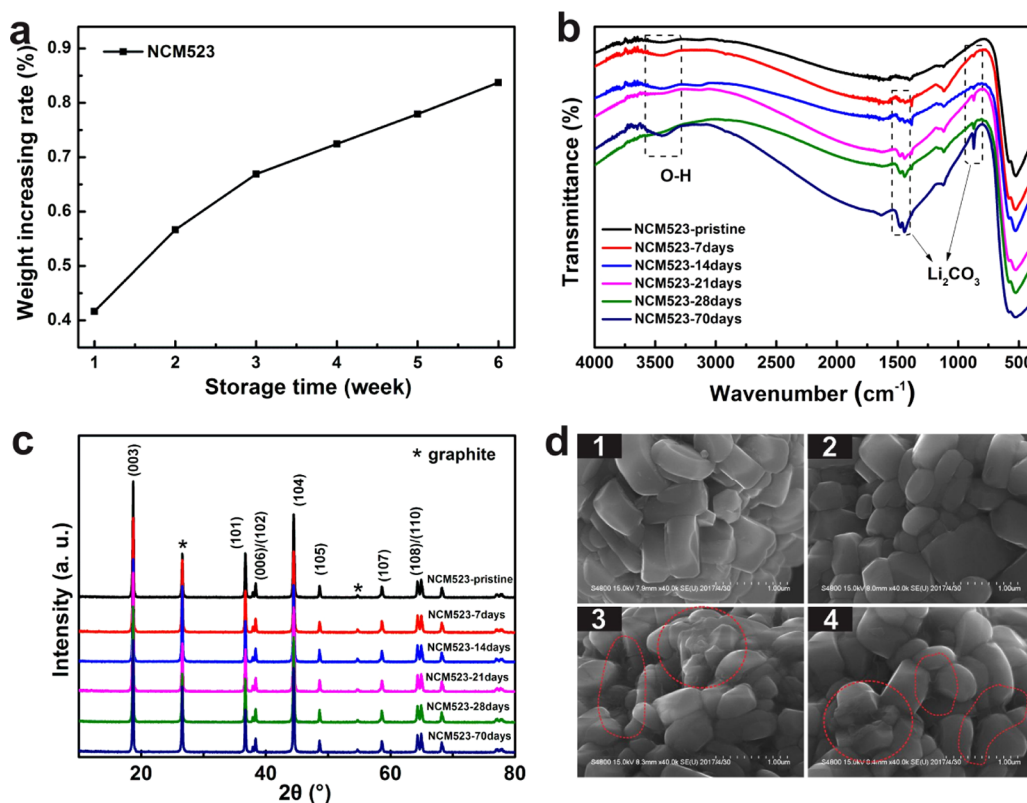


Figure 1. (a) Weight increasing rate of NCM523 with storage time at 55 °C and 80% RH. (b) The FT-IR spectra of the stored and pristine NCM523 materials. (c) XRD figure of the stored and pristine NCM523 materials. (d) SEM images: (1) NCM523-pristine, (2) NCM523-7 days, (3) NCM523-28 days, and (4) NCM523-70 days.

Li_xPO_yF_z (LiF) when stored in the electrolyte (1 M LiPF₆ in 1:1 of ethylene carbonate (EC) and dimethyl carbonate (DMC) solvent) for 4 weeks. Nevertheless, it is generally believed that the NCM cathode materials with high Ni content suffer from sustainable properties and will be coated on a layer of impurities after air exposure. Therefore, it is necessary to study the electrochemical properties of the stored NCM materials and judge the role of Li₂CO₃ in deterioration process both in the materials and the electrochemical performances.

The LiNi_{0.5}Co_{0.2}Mn_{0.3}O₂ (NCM523), one of the most promising NCM cathode materials, has been successfully applied in the commercial lithium-ion batteries.¹⁵ With the widespread application of the NCM523 in the lithium-ion batteries, the direct exposure to air cannot be avoided from the manufacture to the transportation. Thus, we select NCM523 as research feature to study the storage properties of NCM523 for the sake of both the manufacturers and the researchers. In this work, we have systematically studied the electrochemical and thermal properties of NCM523 cathode materials after storage at high-temperature and high-humidity conditions, which is the common weather condition for some of the coastal cities at summer. Our results have revealed that the NCM523 cathode materials exhibited a relatively great storage tolerance against the extreme environmental condition with a little capacity loss in the first cycle and a rapid decline of discharge capacity within the first 10 cycles. The capacity loss in the first cycle can be related to the greater impedance caused by the surface-generated impurity species after the storage at high-temperature and high-humidity conditions, and the surface-generated impurity species continue to affect the subsequent electro-

chemical cycles, leading to a rapid decline in the cycling capacities.

2. EXPERIMENTAL SECTION

2.1. Materials Storage. The LiNi_{0.5}Co_{0.2}Mn_{0.3}O₂ (NCM523) cathode materials were purchased from Beijing Easpring Material Technology Co., Ltd. (China). A chamber (SANTN, China) with controllable temperature and humidity was used to keep the environment at 55 °C and 80% relative humidity (RH) for the storage of the materials. Materials of approximately 5 g were placed into the chamber and were taken out every week to record the weight changes and perform the physical characterization and electrochemical test.

2.2. Physical Characterization. The weight of the NCM523 at different storage times was recorded by an analytical balance (Mettler-Toledo AG, Switzerland). Powder X-ray diffraction (XRD) was performed by Miniflex 600 (Rikagu, Japan), and the operation condition was set up at 40 kV and 15 mA. Testing range was from 10 to 90° at 2°/min¹ with 0.02° step size. Moreover, 6% graphite in mass ratio was ground into the sample to calibrate the peak position before and after storage. The morphologies of NCM523 before and after storage were filmed using a scanning electron microscope (Hitachi Corporation, Japan). Fourier transform infrared (FT-IR) spectra were obtained in transmission mode (using KBr pellet technique) by Xplora (Horiba Corporation, Japan), and the data recording range was from 400 to 4000 cm⁻¹. For differential scanning calorimetry (DSC) test, the NCM523/lithium metal half-cell was charged to 4.30 V and carefully disassembled at an argon-filled glovebox. Before the test, the electrode was washed several times by dimethyl carbonate (DMC) solvent, dried naturally to volatilize the residual solvent, and then the delithiated NCM523 material was cautiously scraped from the current collector. The materials of 3–5 mg and the electrolyte of corresponding amount (material/electrolyte = 1:1 by mg/μL) were added into a stainless sealed pan with a gold-plated cooper seal to

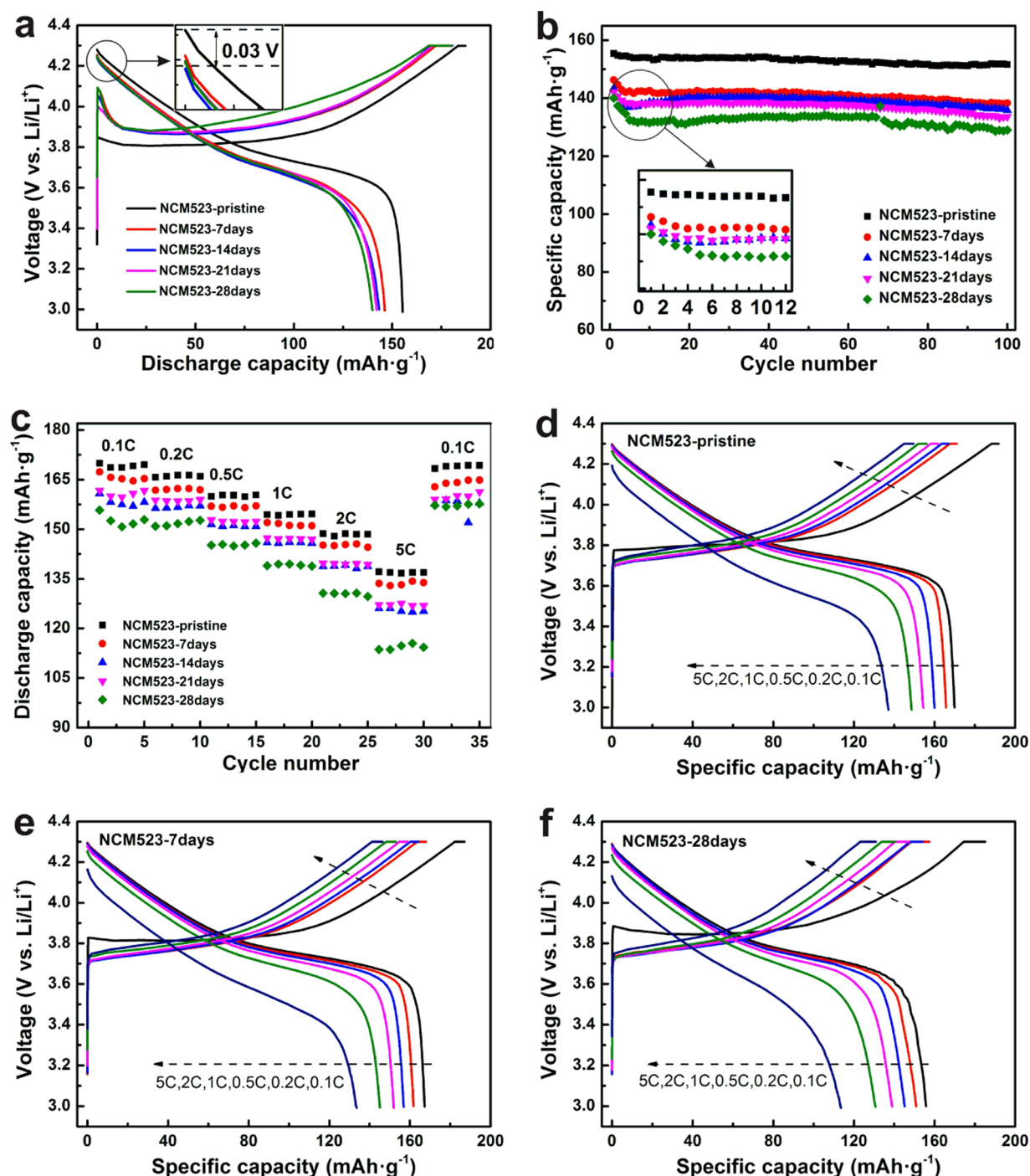


Figure 2. Electrochemical performance of the stored and pristine NCM523 cathode materials: (a) the first charge and discharge profile, (b) cycle performance, and (c) rate performances. The charge and discharge voltage profiles at different rates for (d) NCM523-pristine, (e) NCM523-7 days, and (f) NCM523-28 days.

perform the DSC measurements from 35 to 400 °C in Ar atmosphere by a simultaneous thermal analyzer 449 F1 Jupiter (Netzsch, Germany) and the heating rate was 2 °C/min.

2.3. Electrochemical Measurements. The electrochemical tests were performed on the CR2016-type coin cells with lithium metal as a counter electrode. The NCM523 electrode was made by casting a slurry consisting of 80% NCM523 material, 8% acetylene black, 2% conductive graphite, and 10% poly(vinylidene fluoride) binder (all in mass ratio) dispersed in *N*-methyl-1,2-pyrrolidone solvent onto an aluminum foil using an automatic coating machine. Afterward, the electrode was dried in a vacuum oven at 80 °C overnight. Then, the electrode was punched into a small disc with a radius of 0.6 cm and

the loading density of the disc electrode for all of the electrochemical tests was controlled around 4–5 mg/cm. The coin cells (CR2016) were assembled by sandwiching a separator (Celgard 2400) between the NCM523 electrode and lithium metal counter electrode and using 1 M LiPF₆ electrolyte dissolved in ethylene carbonate (EC) and DMC (volume ratio 1:1) in a glovebox (M. Braun, Germany) filled with argon. The NCM523/lithium metal cells were charged at constant current (CC) and constant voltage mode and discharged at constant current (CC) discharging mode at the voltage range of 3.0–4.3 V by a battery tester (Neware, China). Cyclic voltammetry (CV) measurements were performed on a CHI 1030C (Chenghua, China) electrochemical workstation with a scan rate of 0.1 mV/s in the

potential range of 3.00–4.30 V. Electrochemical impedance spectra (EIS) were recorded on an Autolab PGSTAT101 cell test instrument in the frequency range from 0.1 to 10^5 Hz. All electrochemical data were procured at room temperature.

3. RESULTS AND DISCUSSION

Figure 1 presents the physical and structural properties of the NCM523 materials before and after storage. As shown in Figure 1a, the weight of the material shows a relatively slower growth trend compared to that of $\text{LiNi}_{0.6}\text{Co}_{0.2}\text{Mn}_{0.2}\text{O}_2$ (NCM622) in our previous work.¹⁶ The relation between the weight increasing rate of NCM523 and storage time has also been fitted and presented in Figure S1 accompanied with that of NCM622. Obviously, the NCM523 exhibits a great storage tolerance against the extreme environmental condition with fewer weight increase compared with the NCM622, and it is believed that the Ni^{3+} in NCM makes the material more vulnerable against the attacking from the moisture and the carbon dioxide in air.^{16–18} The FT-IR spectra are shown in Figure 1b. Newly emerging peaks at 1435 and 1496 cm^{-1} are ascribed to the Li_2CO_3 , and absorption peak located at 865 cm^{-1} is derived from the CO_3 group.^{6,19} In addition, the broad bands from 3200 to 3600 cm^{-1} are believed to be derived from LiOH after storage.²⁰ These newly emerging peaks together demonstrate the generation of Li_2CO_3 and LiOH after storage. Furthermore, the increasing intensities of absorption bands at 1435, 1496, and 865 cm^{-1} indicate an increasing amount of Li_2CO_3 in the materials with the storage time. The XRD data of all of the materials (Figure 1c) show an identical structure in $R\bar{3}m$ space group,^{15,21} suggesting that the bulk structure does not change even for longer storage. After stored for 70 days, the (003) position of the NCM523 shifts to the low Bragg angle by around 0.02° (Figure S2a), caused by lithium ions to move out from the primary particles to produce the impurities,^{22–25} such as Li_2CO_3 and LiOH. When lithium ions migrate out from the particles, the electrostatic repulsion between oxygen layers greatly increases because of the unbalance of the regional charge. The weak Bragg diffraction peaks of the NCM523-70 days at 21.26, 30.46, and 31.94 $^\circ$ (Figure S2c) are ascribed to the newly formed crystalline Li_2CO_3 ^{4,6} after storage. Figure 1d shows the scanning electron microscopy (SEM) images of the NCM523 materials before and after storage. The pristine material shows clean and clear primary particles (Figure 1d1), whereas the stored materials (Figure 1d3,d4) show relatively more rough surface, with the junction and accumulation of the primary particles filled with grainy impurities (the red cycle in Figure 1d3,d4), which is believed to be consisted of hydroxide, carbonates, and bicarbonate.^{4,16,26}

Figure 2 gives the cycle and rate performances of NCM523 before and after storage in air. Notably, the first charging plateau of the stored materials overtops that of the pristine materials by 0.05 V, and the discharging plateau is lower than that of the nonstored material about 0.03 V (Figure 2a). According to the previous reports, the foreign matters with inferior ionic/electronic conductivity attached to the surface of the material may isolate some of the active particles, resulting in a higher charge voltage plateau, a lower discharge voltage plateau, and a sudden drop in the initial discharge voltages.^{6,11,21} To figure out the reason why the charging plateau rises along with the storage time, the electrochemical impedance spectroscopic (EIS) measurement has been performed. Figure 3 gives the raw and the fitting data of the

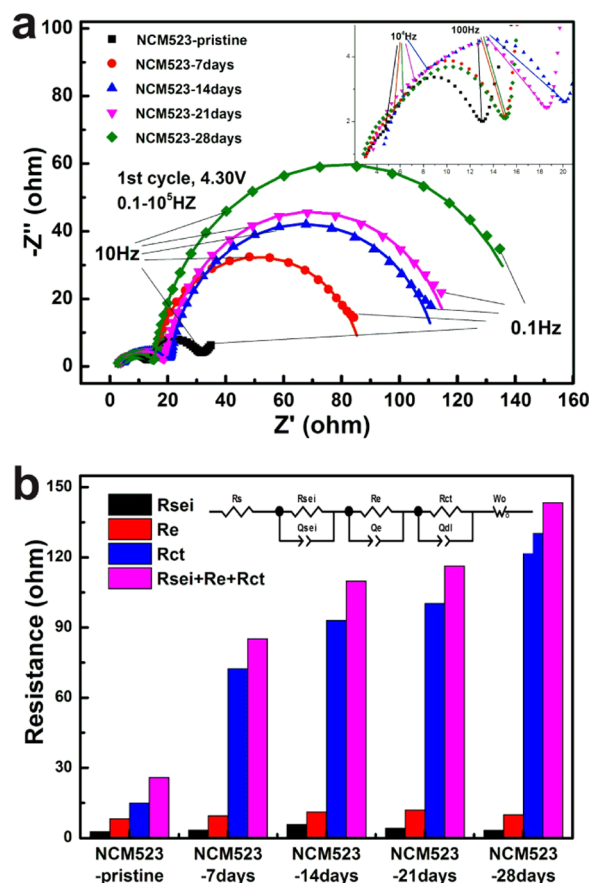


Figure 3. (a) Electrochemical impedance spectroscopy (EIS) profiles and (b) the fitting data of the stored and pristine NCM523 cathode materials.

NCM523 before and after storage at the charged state, and the fitting data are obtained by the Zview software. Clearly, three semicircles, respectively, located at high frequency, high to middle frequency, and middle frequency, appear in the Nyquist plot. According to refs 27–29, the high-frequency semicircle is attributed to the immigration of lithium ions through the solid electrolyte interface (SEI) film coated on the surface of NCM523 particles, the middle-frequency semicircle is related to the charge transfer through the electrode/electrolyte interface, and the high- to middle-frequency semicircle is corresponding to the electronic properties of the materials, which is involved in the conductive materials, the binder, the active materials, the SEI films covered on the surface of the active materials, and the contact among particles and conductive materials. The equivalent circuit is inserted into Figure 3b, where the R_{sei} represents the resistance of SEI films, the R_e stands for the electronic resistance of the material, and the R_{ct} is the resistance of charge transfer reaction.²⁷ With storage time prolonging, either R_{sei} or R_e shows few changes but the R_{ct} grows sharply after storage and contributes to the most increase of the total resistance. As aforementioned, the R_{ct} represents the charge transfer impedance at the electrode/electrolyte interface, and the materials surface is covered with a layer of low ionically/electronically conductive impurities after storage. Thus, we believe that the impurities covered on the surface of the materials after 4 weeks storage, less than 0.8% in mass ratio, significantly lead to the impedance or the charging plateau increase of the stored materials.

According to ref 29, the Li_2CO_3 films are replaced by other surface films composed of a variety of species formed by interaction between the active materials and electrolyte upon cycling. And upon storage in the electrolyte (LiPF_6 in EC–DMC),^{14,30} the Li_2CO_3 will be slowly transformed into LiF and other species, which further increases the surface impedance of the materials. After storage in the air, the complicated impurities covered on the surface of the NCM materials may further react with the electrolyte, making the traditional perspective of the mainly deteriorated effect of Li_2CO_3 different. To verify whether the reaction between the impurities generated after storage and the electrolyte occurs or not, the NCM523-pristine, NCM523-28 days, and NCM523-70 days are put into the electrolyte for 24 h and then taken out for test after drying in a vacuum oven. Figure 4 presents the

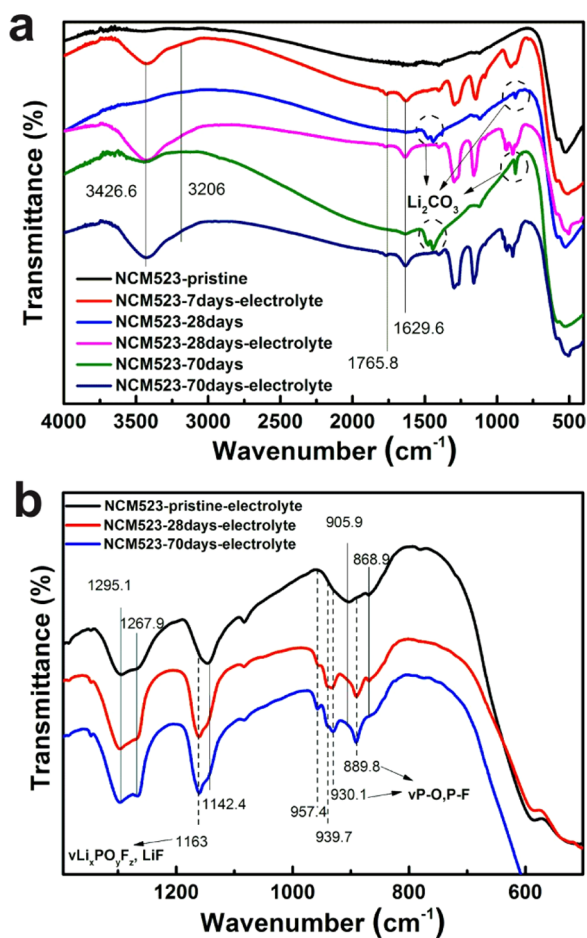


Figure 4. (a) FT-IR of the NCM523-pristine, NCM523-28 days, and NCM523-70 days before and after stored in electrolyte for 24 h and (b) enlarged profiles between 500 and 1400 cm^{-1} .

FT-IR spectra before and after storage in the electrolyte for the NCM523-pristine, NCM523-28 days, and NCM523-70 days. For the NCM523-28 days and NCM523-70 days, the absorption peaks of CO_3^{2-} at 1435, 1496, and 865 cm^{-1} surprisingly disappeared after stored in the electrolyte, whereas the peaks at 3206 and 3426 cm^{-1} increased a lot, which are previously assigned to the LiPF_6 compound and O–H stretching vibrations.^{29,30} In addition, a few absorption peaks appear at range of 800–1200 cm^{-1} , as presented in Figure 4b. In the spectra of NCM523-28 days and NCM523-70 days, new bands emerged at 889.8 and 930.1 cm^{-1} , which correspond to

the P–O or P–F vibration,³¹ and the band at 1163 cm^{-1} is ascribed to the vibration in the compound $\text{Li}_x\text{PO}_y\text{F}_z$ or LiF.^{30,31} The new modes at 939.7 and 957.4 cm^{-1} may be related to the vibration of C=O or O–C=O based on some references.²⁹ While for the pristine NCM523, these bands do not appear. These all suggest that the impurities generated after storage at 55 °C and 80% RH will react with the electrolyte and form new impurities shrouding the surface of the materials, i.e., $\text{Li}_x\text{PO}_y\text{F}_z$, LiF, and species containing C=O or O–C=O. The redundant $\text{Li}_x\text{PO}_y\text{F}_z$ and LiF rapidly created, we think, are derived from the reaction between the impurities, e.g., Li_2CO_3 , LiOH, bicarbonate, and LiPF_6 , and the species containing C=O or O–C=O definitely come from the decomposition of the solvent, i.e., EC–DMC. Both the inorganic components ($\text{Li}_x\text{PO}_y\text{F}_z$ or LiF, Li_2CO_3 , LiOH) and the organic species (species containing C=O or O–C=O) are badly electronic conductor,^{32,33} consequently resulting in a high-charge potential platform and a low-discharge potential platform. And this is why the charging plateau of the stored materials overtops that of the nonstored materials from the outset of charging.

In Figure 2b, the cycle discharge capacities of NCM523 after storage exhibit a small decay in the first 10 cycles and then maintain stability in the following 90 cycles, whereas the discharge capacities of pristine NCM523 do not decrease obviously in the total cycles. The charge/discharge voltage profiles of the NCM523-pristine and NCM523-28 days in the first 10 cycles are plotted in Figure S3a,b, and the coulombic efficiencies (CEs) of the total cycles are given in Figure S3c,d. Evidently, the charge and discharge potential curves of different cycles of NCM523-pristine almost overlap at 3.0–4.3 V, whereas those of NCM523-28 days do not overlap due to the increasing overpotential, indicating that more surface species with low electronic/ionic conductivity cover the particles of sample NCM523-28 days with cycles. The coulombic efficiencies of all of the pristine and stored materials nearly approach to 100% since the second cycle, and the CE of the first cycle decreases with the storage time increasing, indicating that the parasitic reactions related to the formation of solid electrode interface (SEI) inevitably increase at the surface of the cathode materials.^{34,35} To find out if there is a new electrochemical reaction resulting in capacity fading for the stored materials, the cyclic voltammetry (CV) tests are carried out, as described in Figure 5. For the pristine and stored materials, there are only one oxidation peak at around 3.90 V and one reduction peak at around 3.70 V, which are respectively corresponding to the deintercalation and intercalation of lithium ions,^{36,37} without any new redox reactions emerging. However, the oxidation peak shifts to a high potential and the reduction peak shifts to a low potential for the storage materials at the first cycle. In the subsequent cycles, the oxidation peaks of the stored materials shift back to a low potential but that of the pristine material almost stay at the same position with only few shifts. For the NCM523-pristine, the oxidation peak moves from 3.86 to 3.84 V at the second cycle and then moves back to 3.85 V at the fifth cycle. For NCM523-7 days, the anodic peak potential of the first cycle located at 3.90 V moves to 3.845 V (second cycle) and then back to 3.86 V (fifth cycle). For the NCM523-28 days, that is from 3.97 V (first cycle) to 3.87 V (second cycle) and then to 3.86 V (fifth cycle). At the fifth cycle, the oxidation peaks of all of the samples almost move to the same position. The first anodic peak located at a higher voltage than that of the

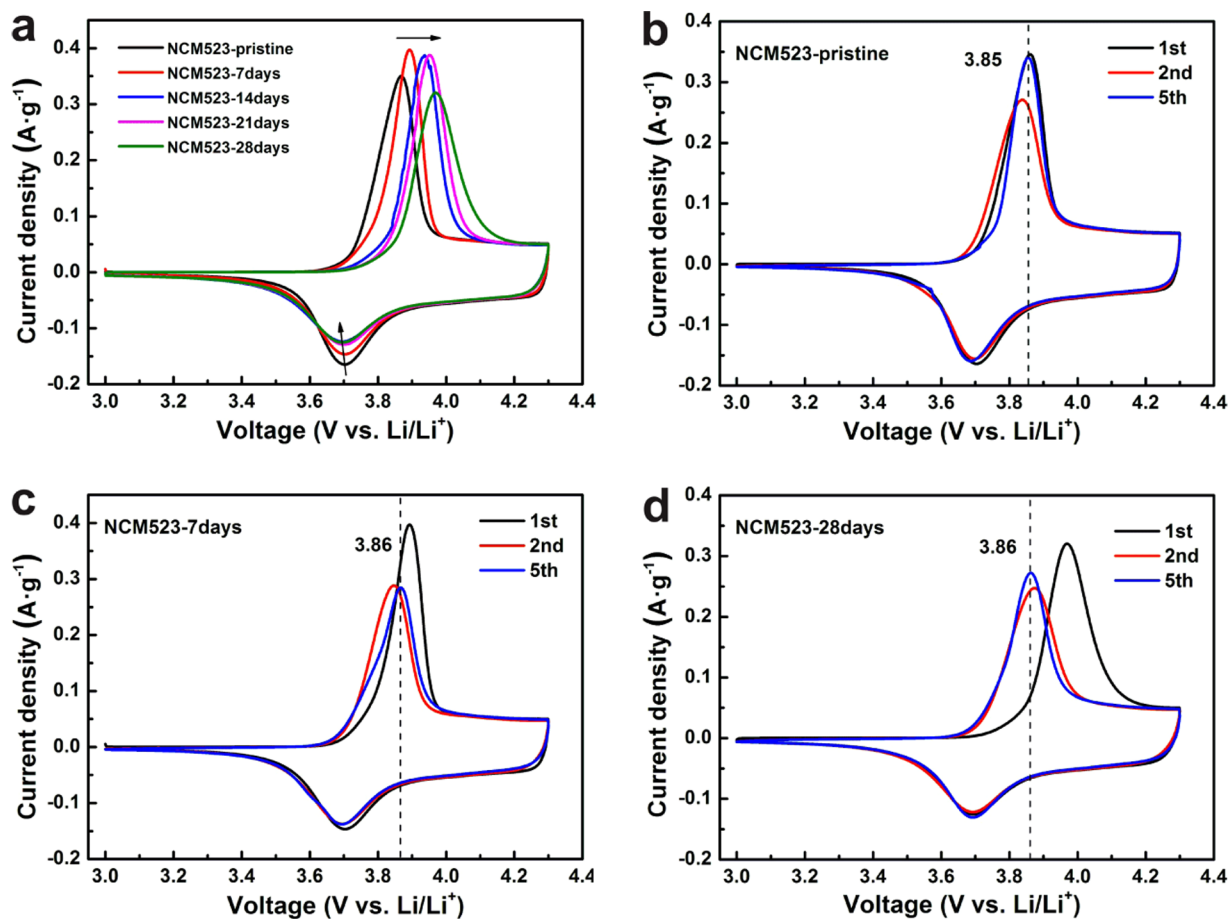


Figure 5. Cyclic voltammograms: (a) the first cycle for the pristine and stored NCM523 materials, (b) the NCM523-pristine, (c) NCM523-7 days, and (d) NCM523-28 days.

subsequent cycles was related to the formation of a layer of SEI, and the shifts back to lower voltage would be completed by the fifth cycle.^{38–40} Undoubtedly, the anodic peak potential of the first cycle of the pristine material shows a slightly higher voltage, which is related to the formation process of SEI, whereas that of the stored materials presents a hugely higher potential, which should be the integrated result of the SEI formation and the chemical reaction before the charging process. As abovementioned, the new inorganic components ($\text{Li}_x\text{PO}_y\text{F}_z$ or LiF) and the organic species (species containing $\text{C}=\text{O}$ or $\text{O}-\text{C}=\text{O}$ groups) are produced at the first touch between the impurities and the electrolyte through the specific chemical reaction, causing a huge overpotential, which may be the major reason for the oxidation peak shifting to higher potentials. Besides, the quickly shifting back of oxidation peak in the following cycles for the stored materials shares the same mechanism as that of the pristine materials to form a stable interface between the electrode and the electrolyte.

Figure 6 presents the dynamic changes of the impedances of the pristine and stored materials along with cycles. The equivalent circuits of successive lines in Figure 6a,c,e are presented in Figure 3b. As can be seen, the fitting lines are in well accordance with the experimental points. The R_{sei} of all three batteries, which represent the resistances of lithium ions migrating through SEI films, does not show obvious changes even at the 70th cycle (varying from 2.7 to 4.7 Ω for NCM523-pristine, 3.3 to 6.0 Ω for NCM523-28 days, and 23.3 to 18.5 Ω for NCM523-70 days). The low and stable value of R_{sei} with

cycles indicates that the minimally formed and fairly stable surface films protect the NCM523 electrode materials against the electrolyte,⁴¹ even for the stored materials. Also, the minor augment of R_{sei} illustrates the modest gain in quantity of SEI with continuous cycles. The R_e denoting the conductivity of the electrode²⁷ also fluctuates a little for NCM523-pristine (8.2–10.1 Ω) and NCM523-28 days (10.0–11.6 Ω) after 70 cycles but increases a lot for the sample NCM523-70 days (11.7–40.9 Ω), indicating that the contact among active particles and conductive agent worsens after repeated cycle. The R_{cv} derived from the charge-transfer process at the interface between the electrode particles and the electrolyte,⁴¹ shows a significant evolution for the storage samples and is stable for the nonstored sample along with the cycles. The R_{ct} of the NCM523-28 days doubles during the first three cycles, varying from 130.2 to 261 Ω , and quickly drops until the 10th cycle (83.8 Ω), and then gradually increases, reaching 264.5 Ω at the 70th cycles, indicating a changing lithium-ion diffusion coefficient in the material and/or the electrode kinetics.⁴¹ Similarly, the NCM523-70 days give the same trend of the evolution of R_{ct} along with cycles. However, the R_{ct} of the pristine NCM523 sample only slightly fluctuates in the first four cycles with the variation less than 7 Ω . Interestingly, the fast variations of R_{ct} exactly corresponds to the rapid attenuation of the specific discharge capacity in the first 10 cycles of the storage sample in Figure 2b, and the correlations between the two are discussed below.

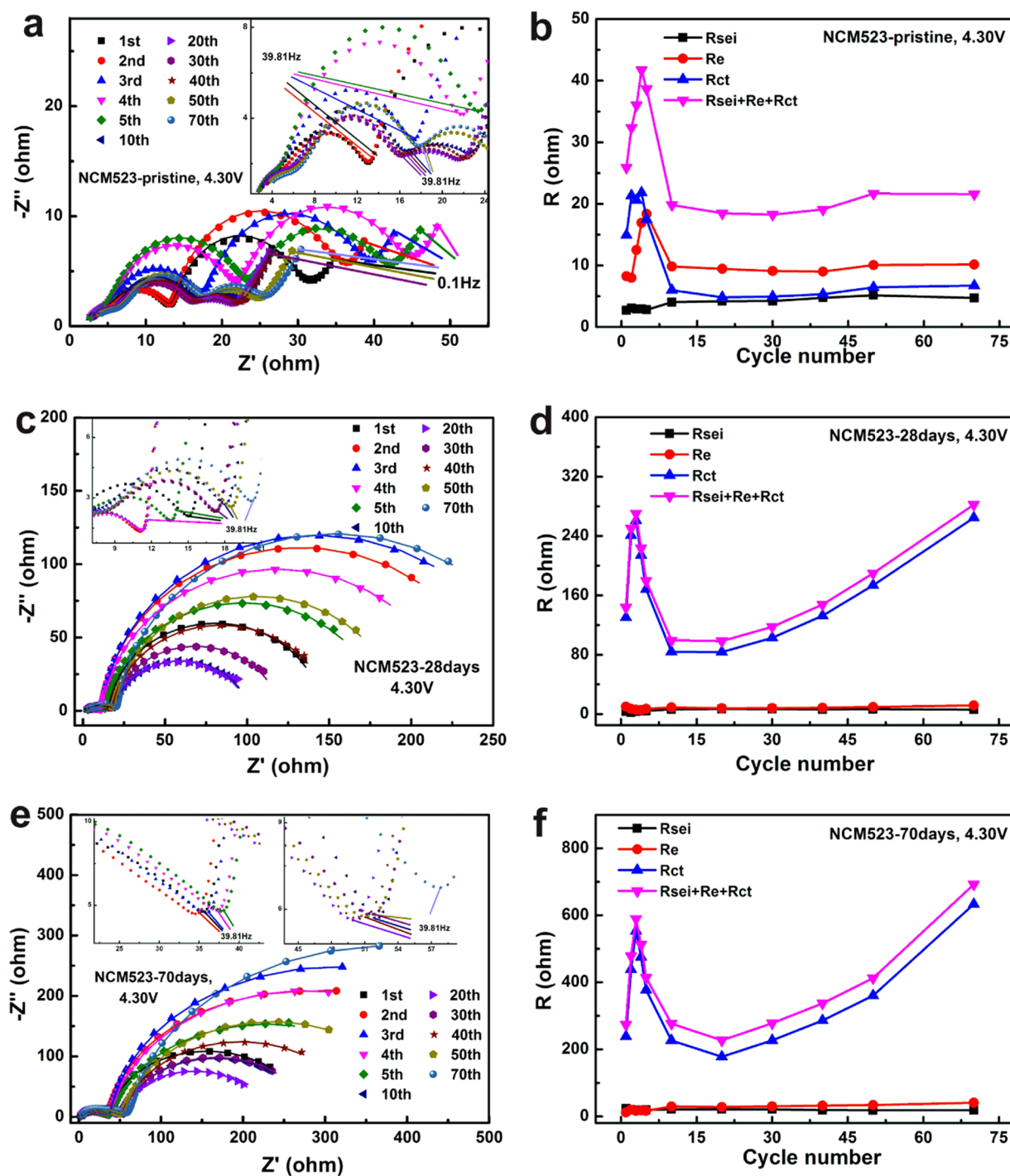


Figure 6. Nyquist plots and fitting curves at series of cycles: (a) NCM523-pristine, (c) NCM523-28 days, and (e) NCM523-70 days. The successive variation of fitting data: (b) NCM523-pristine, (d) NCM523-28 days, and (f) NCM523-70 days.

Figure 7 gives the initial discharge potentials of the pristine and stored materials, obtained from the discharge data in Figures 2a,b and S4. Notably, the initial discharge potentials of the stored materials at the first 10 cycles show significant voltage waving and continuously attenuate after 10 cycles in contrast to the pristine NCM523 material. Moreover, the initial discharge potentials of the first 10 cycles for the stored materials, which show a sudden drop in the first three or four cycles but quick return within the 10th cycle, change oppositely against the R_{ct} with cycles, revealing that the initial discharge potentials can be directly intervened by the

impedance of charge-transfer process during the lithiated and delithiated process and indirectly reflect the delithiation degree of the cathode materials at the end of the charge process. Therefore, the fast waving intervals of R_{ct} in the first 10 cycles directly constrain the initial discharge potential at the same charge/discharge cut-off condition and further result in the discharge capacity instantly decreasing, as depicted in Figure 2b and aforementioned description.

To verify above conclusion, the electrochemical performances of the stored and pristine materials are again measured at low charge/discharge current. In this regard, the hindered

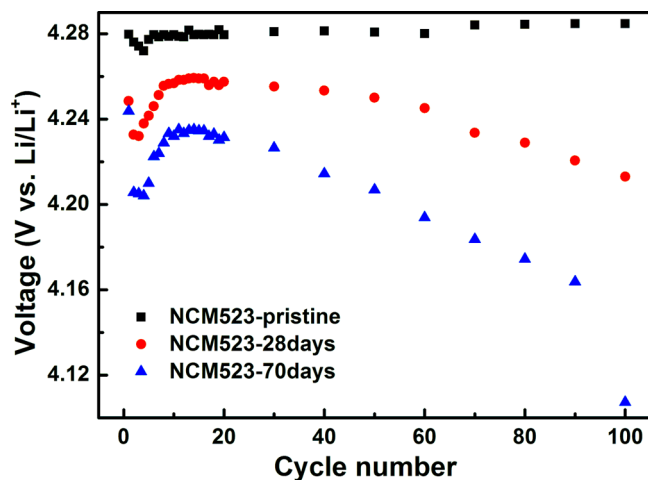


Figure 7. Initial discharge potential of the NCM523-pristine, NCM523-28 days, and NCM523-70 days after charged to 4.3 V at successive cycles.

electrode kinetics caused by the larger charge-transfer impedance after the storage is largely impaired, as shown in Figures 8 and S5. The great enhancement of the first discharge capacity and CE (Figure 8a) with the decreasing charge/discharge rates reveals that the sluggish kinetics involving the low lithium-ion and electrons conductivity get enormously

relieved especially at low charge/discharge current. Also, the charging plateau decreases and the discharging plateau increases at the low charge/discharge rate (Figure 8b) due to the minor polarization.⁴² For the sample NCM523-28 days, although it has a slight decrease in first three cycles and a relatively lower discharge capacity compared to the NCM523-pristine, the electrochemical discharge capacity gets slow recovery at 0.1 and 0.2 C (1 C = 160 mA/g) charge/discharge current within 10 cycles and then stabilize, whereas the discharge capacity at 0.5 C current also decreases in the first 10 cycles, indicating that the stored materials at the testing current more than 0.5 C cannot recover the electrochemical discharge capacity due to the fast changing interval of R_{ct} in the first 10 cycles.

Figure 2c,f presents the rate discharge performances of the materials. Obviously, with the extension of the storage time, the rate performances of the stored materials get deteriorated, especially at the large discharge rate, which is believed to be hindered by the impurities generated after storage and the reactions between the impurities and the electrolyte.

The thermal stability of the stored and pristine NCM523 materials (charged to 4.3 V) is studied by the differential scanning calorimetry (DSC) and thermogravimetry test, as shown in Figure 9. Two exothermic peaks, located at around 275 and 302 °C, are observed. The exothermic peak at 275 °C is attributed to the oxidation reaction between the delithiated materials and the electrolyte and the decomposition reaction of

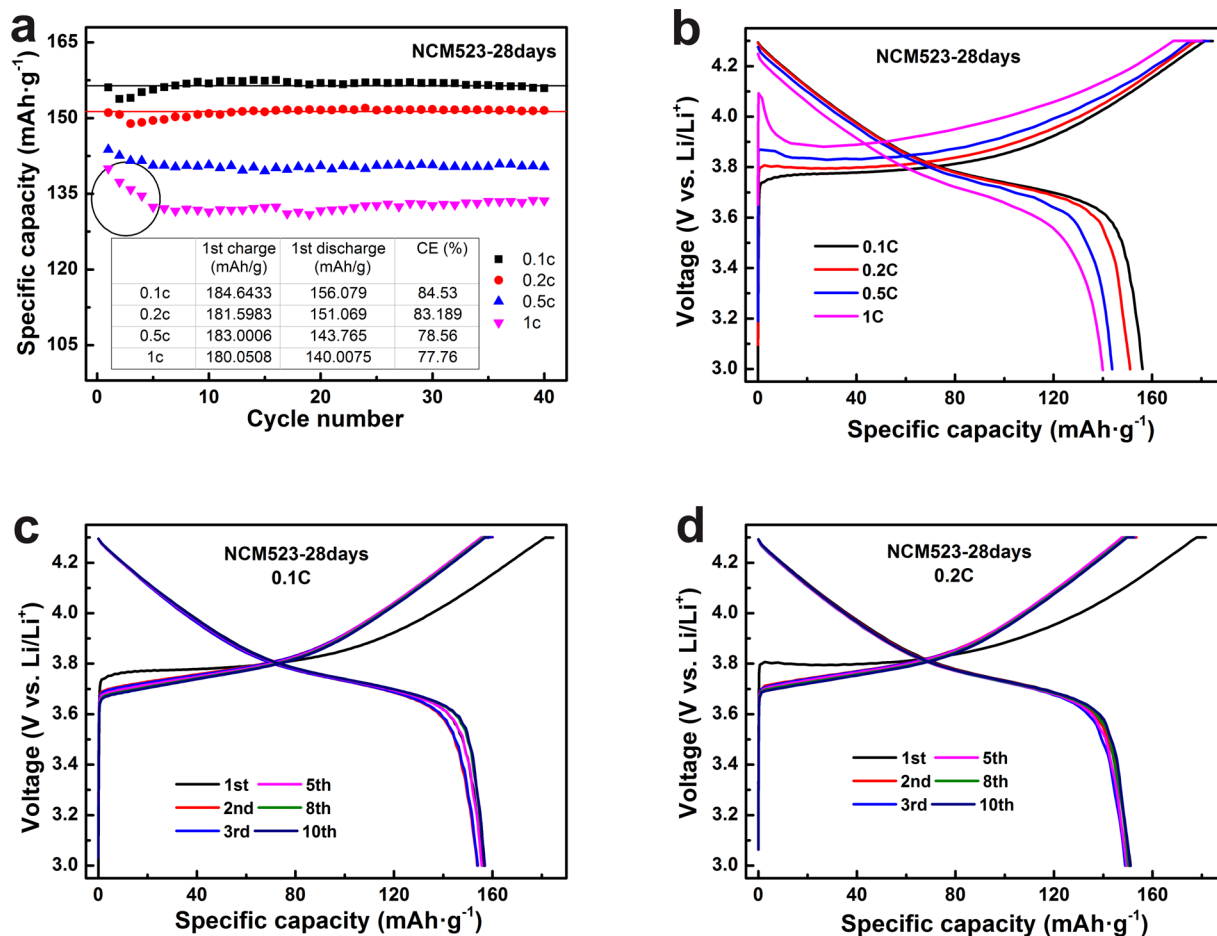


Figure 8. (a) Specific discharge capacity and (b) first charge/discharge profiles of the NCM523-28 days at 1, 0.5, 0.2, and 0.1 C (1 C = 160 mA/g); the charge/discharge profiles at (c) 0.1 C and (d) 0.2 C of NCM523-28 days.

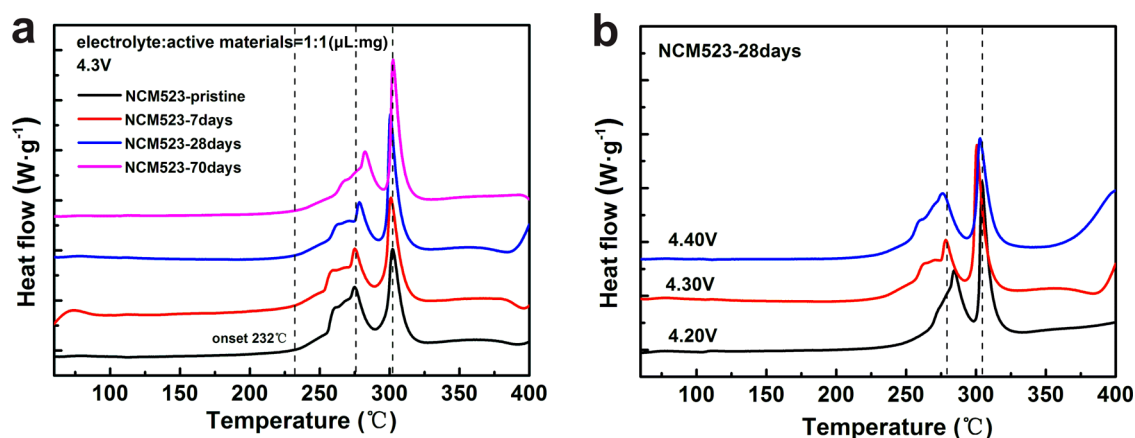


Figure 9. DSC profiles: (a) pristine and stored NCM523 materials after charged to 4.3 V and (b) NCM523-28 days after charged to 4.2 and 4.4 V.

electrolyte itself,^{43,44} and the one at 302 °C is owing to the oxidizing of solvents by oxygen released from the delithiated materials.^{43,45,46} With the storage time increasing, the first exothermic peak moves to the higher temperature, whereas the second exothermic peak keeps the temperature position with a slightly increasing maximal heat flow (Table S1). The NCM523 materials are coated by a layer of impurities consisting of easily decomposed adsorbed species and hard-decomposed Li_2CO_3 and LiOH ¹⁶ after storage, and the impurities will further react with the electrolyte to generate new low electron/lithium-ion conductivity impurities, such as $\text{Li}_x\text{PO}_y\text{F}_z$ (LiF , organic species containing $\text{C}=\text{O}$ or $\text{O}-\text{C}=\text{O}$), covered on the surface of the materials (Figure 4), causing a higher impedance and charge potential plateau. Thus, the delithiated state of the stored materials after being charged to 4.3 V is absolutely lower than that of the pristine materials. As mentioned above, the first exothermic peak is partly related to the reaction of the delithiated materials and the electrolyte, therefore the delithiated state of the materials determines the temperature position of the first exothermic peak to some extent. To verify our point of view, the thermal behaviors of NCM523-28 days charged to 4.2 or 4.4 V with the same charging mode are tested, as shown in Figure 9b. The first exothermic peak of the sample charged 4.2 V moves to a high temperature, whereas that of the sample charged to 4.4 V moves to a low temperature. Thus, the slightly better thermal behavior of the stored materials is ascribed to the lower delithiated state, caused by the higher impedance impurities generated in the air storage and the reactions of the impurities and the electrolyte in the batteries, at the same charging mode.

4. CONCLUSIONS

To sum up, we have systematically studied the effects of extreme storage condition on the physical properties and electrochemical performances of NCM523 materials. After stored at 55 °C and 80% RH, the NCM523 materials are coated by a layer of impurities consisting of the adsorbed species, Li_2CO_3 and LiOH , inevitably resulting in the mass gain. When the stored NCM523 materials serve as the cathode materials in the lithium-ion batteries, the impurities generated in the air exposure quickly react with the electrolyte and promptly turn into new inorganic components ($\text{Li}_x\text{PO}_y\text{F}_z$ or LiF) and organic species (species containing $\text{C}=\text{O}$ or $\text{O}-\text{C}=\text{O}$ groups), causing a higher impedance and charge potential plateau. Furthermore, the discharge capacity of the stored

NCM523 electrode quickly declines in the first 10 cycles at high rates (≥ 0.5 C) owing to a larger and changeable electrochemical impedance, and this phenomenon disappears at low charging/discharging current (≤ 0.2 C). In addition, the thermal stability of the stored NCM523 materials getting slightly better is due to the relatively lower delithiated state at the charged states, which is caused by the superficial higher impedance impurities.

■ ASSOCIATED CONTENT

Supporting Information

The Supporting Information is available free of charge on the ACS Publications website at DOI: 10.1021/acsami.8b07873.

The linear fitting profiles of the weight increasing rate (W) and the square root of storage time ($t^{1/2}$) for the NCM523 and the NCM622 (Figure S1); partially enlarged XRD patterns (Figure S2); the initial charge and discharge voltage profiles (Figure S3); the specific discharge capacity of the NCM523-pristine, the NCM523-28 days, and the NCM523-70 days (Figure S4); the specific discharge capacity and first charge/discharge profiles of the NCM523-pristine at 0.1, 0.2, and 1 C (1 C = 160 mA/g) (Figure S5); and the thermodynamic data of the pristine and stored NCM523 samples after being charged to 4.3 V with electrolyte (Table S1) (PDF)

■ AUTHOR INFORMATION

Corresponding Authors

*E-mail: wangjing2015@xmu.edu.cn (J.W.).

*E-mail: jbzhaoh@xmu.edu.cn (J.Z.).

ORCID

Jinbao Zhao: 0000-0002-2753-7508

Notes

The authors declare no competing financial interest.

■ ACKNOWLEDGMENTS

This work is financially supported by National Natural Science Foundation of China (21603179), the Fundamental Research Funds for the Central Universities (20720170021), National Natural Science Foundation of China (21621091), National Key Research and Development Program of China (2017YFB0102000), and National Fund for Fostering Talents of Basic Science (J1310024). The authors also wish to express

their gratitude to Prof. Daiwei Liao for his valuable suggestions.

REFERENCES

- (1) Manthiram, A.; Knight, J. C.; Myung, S.-T.; Oh, S.-M.; Sun, Y.-K. Nickel-Rich and Lithium-Rich Layered Oxide Cathodes: Progress and Perspectives. *Adv. Energy Mater.* **2016**, *6*, No. 1501010.
- (2) Liu, W.; Oh, P.; Liu, X.; Lee, M. J.; Cho, W.; Chae, S.; Kim, Y.; Cho, J. Nickel-rich layered lithium transition-metal oxide for high-energy lithium-ion batteries. *Angew. Chem., Int. Ed.* **2015**, *54*, 4440–4457.
- (3) Bak, S. M.; Hu, E.; Zhou, Y.; Yu, X.; Senanayake, S. D.; Cho, S. J.; Kim, K. B.; Chung, K. Y.; Yang, X. Q.; Nam, K. W. Structural changes and thermal stability of charged $\text{LiNi}_x\text{Mn}_y\text{Co}_z\text{O}_2$ cathode materials studied by combined in situ time-resolved XRD and mass spectroscopy. *ACS Appl. Mater. Interfaces* **2014**, *6*, 22594–22601.
- (4) Liu, H.; Yang, Y.; Zhang, J. Investigation and improvement on the storage property of $\text{LiNi}_{0.8}\text{Co}_{0.2}\text{O}_2$ as a cathode material for lithium-ion batteries. *J. Power Sources* **2006**, *162*, 644–650.
- (5) Liu, H.; Yang, Y.; Zhang, J. Reaction mechanism and kinetics of lithium ion battery cathode material LiNiO_2 with CO_2 . *J. Power Sources* **2007**, *173*, 556–561.
- (6) Zhuang, G. V.; Chen, G.; Shim, J.; Song, X.; Ross, P. N.; Richardson, T. J. Li_2CO_3 in $\text{LiNi}_{0.8}\text{Co}_{0.15}\text{Al}_{0.05}\text{O}_2$ cathodes and its effects on capacity and power. *J. Power Sources* **2004**, *134*, 293–297.
- (7) Eom, J.; Kim, M. G.; Cho, J. Storage Characteristics of $\text{LiNi}_{0.8}\text{Co}_{0.1+x}\text{Mn}_{0.1-x}\text{O}_2$ ($x = 0, 0.03$, and 0.06) Cathode Materials for Lithium Batteries. *J. Electrochem. Soc.* **2008**, *155*, A239–A245.
- (8) Zhao, Y.; Wang, S.; Ren, W.; Wu, R. Storage Characteristics and Surface Basicity Properties of Li-Rich Cathode Materials Used in Lithium Ion Batteries. *J. Electrochem. Soc.* **2013**, *160*, A82–A86.
- (9) Shi, J. L.; Qi, R.; Zhang, X. D.; Wang, P. F.; Fu, W. G.; Yin, Y. X.; Xu, J.; Wan, L. J.; Guo, Y. G. High-Thermal- and Air-Stability Cathode Material with Concentration-Gradient Buffer for Li-Ion Batteries. *ACS Appl. Mater. Interfaces* **2017**, *9*, 42829–42835.
- (10) Grenier, A.; Liu, H.; Wiaderek, K. M.; Lebens-Higgins, Z. W.; Borkiewicz, O. J.; Piper, L. F. J.; Chupas, P. J.; Chapman, K. W. Reaction Heterogeneity in $\text{LiNi}_{0.8}\text{Co}_{0.15}\text{Al}_{0.05}\text{O}_2$ Induced by Surface Layer. *Chem. Mater.* **2017**, *29*, 7345–7352.
- (11) Lebens-Higgins, Z. W.; Sallis, S.; Faenza, N. V.; Badway, F.; Pereira, N.; Halat, D. M.; Wahila, M.; Schlueter, C.; Lee, T.-L.; Yang, W.; Grey, C. P.; Amatucci, G. G.; Piper, L. F. J. Evolution of the Electrode–Electrolyte Interface of $\text{LiNi}_{0.8}\text{Co}_{0.15}\text{Al}_{0.05}\text{O}_2$ Electrodes Due to Electrochemical and Thermal Stress. *Chem. Mater.* **2018**, *30*, 958–969.
- (12) Shi, S.; Qi, Y.; Li, H.; Hector, L. G. Defect Thermodynamics and Diffusion Mechanisms in Li_2CO_3 and Implications for the Solid Electrolyte Interphase in Li-Ion Batteries. *J. Phys. Chem. C* **2013**, *117*, 8579–8593.
- (13) Ling, C.; Zhang, R.; Takechi, K.; Mizuno, F. Intrinsic Barrier to Electrochemically Decompose Li_2CO_3 and LiOH . *J. Phys. Chem. C* **2014**, *118*, 26591–26598.
- (14) Bi, Y.; Wang, T.; Liu, M.; Du, R.; Yang, W.; Liu, Z.; Peng, Z.; Liu, Y.; Wang, D.; Sun, X. Stability of Li_2CO_3 in cathode of lithium ion battery and its influence on electrochemical performance. *RSC Adv.* **2016**, *6*, 19233–19237.
- (15) Jung, S.-K.; Gwon, H.; Hong, J.; Park, K.-Y.; Seo, D.-H.; Kim, H.; Hyun, J.; Yang, W.; Kang, K. Understanding the Degradation Mechanisms of $\text{LiNi}_{0.5}\text{Co}_{0.2}\text{Mn}_{0.3}\text{O}_2$ Cathode Material in Lithium Ion Batteries. *Adv. Energy Mater.* **2014**, *4*, No. 1300787.
- (16) Chen, Z.; Wang, J.; Huang, J.; Fu, T.; Sun, G.; Lai, S.; Zhou, R.; Li, K.; Zhao, J. The high-temperature and high-humidity storage behaviors and electrochemical degradation mechanism of $\text{LiNi}_{0.6}\text{Co}_{0.2}\text{Mn}_{0.2}\text{O}_2$ cathode material for lithium ion batteries. *J. Power Sources* **2017**, *363*, 168–176.
- (17) Matsumoto, K.; Kuzuo, R.; Takeya, K.; Yamanaka, A. Effects of CO_2 in air on Li deintercalation from $\text{LiNi}_{1-x}\text{Co}_x\text{Al}_y\text{O}_2$. *J. Power Sources* **1999**, *81*–*82*, 558–561.
- (18) Shizuka, K.; Kiyohara, C.; Shima, K.; Okahara, K.; et al. ECS-Effect of CO_2 on Layered $\text{Li}_{1+z}\text{Ni}_{1-x}\text{Co}_x\text{M}_y\text{O}_2$ ($M = \text{Al}, \text{Mn}$) Cathode Materials. *ECS Trans.* **2008**, *11*, 7–13.
- (19) Ostrovskii, D.; Ronci, F.; Scrosati, B.; Jacobsson, P. Reactivity of lithium battery electrode materials toward non-aqueous electrolytes: spontaneous reactions at the electrode-electrolyte interface investigated by FTIR. *J. Power Sources* **2001**, *103*, 10–17.
- (20) Xiong, X.; Wang, Z.; Yue, P.; Guo, H.; Wu, F.; Wang, J.; Li, X. Washing effects on electrochemical performance and storage characteristics of $\text{LiNi}_{0.8}\text{Co}_{0.1}\text{Mn}_{0.1}\text{O}_2$ as cathode material for lithium-ion batteries. *J. Power Sources* **2013**, *222*, 318–325.
- (21) Zhang, X.; Jiang, W. J.; Zhu, X. P.; Mauger, A.; Qilu, Julien, C. M. Aging of $\text{LiNi}_{1/3}\text{Mn}_{1/3}\text{Co}_{1/3}\text{O}_2$ cathode material upon exposure to H_2O . *J. Power Sources* **2011**, *196*, 5102–5108.
- (22) Reimers, J. N.; Dahn, J. N. Electrochemical and In Situ X-ray Diffraction Studies of Lithium Intercalation in Li_xCoO_2 . *J. Electrochem. Soc.* **1992**, *139*, 2091–2097.
- (23) Li, W.; Dahn, J. R.; Reimers, J. In situ X-ray diffraction and electrochemical studies of $\text{Li}_{1-x}\text{NiO}_2$. *Solid State Ionics* **1993**, *67*, 123–130.
- (24) Balasubramanian, M.; Sun, X.; Yang, X. Q.; McBreen, J. In situ X-ray diffraction and X-ray absorption studies of high-rate lithium-ion batteries. *J. Power Sources* **2001**, *92*, 1–8.
- (25) Dolotko, O.; Senyshyn, A.; Mühlbauer, M. J.; Nikolowski, K.; Ehrenberg, H. Understanding structural changes in NMC Li-ion cells by in situ neutron diffraction. *J. Power Sources* **2014**, *255*, 197–203.
- (26) Oh, P.; Song, B.; Li, W.; Manthiram, A. Overcoming the chemical instability on exposure to air of Ni-rich layered oxide cathodes by coating with spinel $\text{LiMn}_{1.9}\text{Al}_{0.1}\text{O}_4$. *J. Mater. Chem. A* **2016**, *4*, 5839–5841.
- (27) Zhuang, Q.; Wei, T.; Du, L.; Cui, Y.; Fang, L.; Sun, S. An Electrochemical Impedance Spectroscopic Study of the Electronic and Ionic Transport. *J. Phys. Chem. C* **2010**, *114*, 8614–8621.
- (28) Zhao, X.; Zhuang, Q.-C.; Wu, C.; Wu, K.; Xu, J.-M.; Zhang, M.-Y.; Sun, X.-L. Impedance Studies on the Capacity Fading Mechanism of $\text{LiNi}_{0.5}\text{Co}_{0.2}\text{Mn}_{0.3}\text{O}_2$ Cathode with High-Voltage and High-Temperature. *J. Electrochem. Soc.* **2015**, *162*, A2770–A2779.
- (29) Aurbach, D.; Gamolsky, K.; et al. The Study of Surface Phenomena Related to Electrochemical Lithium Intercalation into Li_xMO_y Host Materials ($M = \text{Ni}, \text{Mn}$). *J. Electrochem. Soc.* **2000**, *147*, 1322–1331.
- (30) Ostrovskii, D.; Ronci, F.; Scrosati, B.; Jacobsson, P. Reactivity of lithium battery electrode materials toward non-aqueous electrolytes: spontaneous reactions at the electrode-electrolyte interface investigated by FTIR. *J. Power Sources* **2001**, *103*, 10–17.
- (31) Ostrovskii, D.; Ronci, F.; Scrosati, B.; Jacobsson, P. A FTIR and Raman study of spontaneous reactions occurring at the $\text{Li-Ni}_y\text{Co}_{(1-y)}\text{O}_2$ electrode/non-aqueous electrolyte interface. *J. Power Sources* **2001**, *94*, 183–188.
- (32) Wang, X.; Zhang, M.; Alvarado, J.; Wang, S.; Sina, M.; Lu, B.; Bouwer, J.; Xu, W.; Xiao, J.; Zhang, J. G.; Liu, J.; Meng, Y. S. New Insights on the Structure of Electrochemically Deposited Lithium Metal and Its Solid Electrolyte Interphases via Cryogenic TEM. *Nano Lett.* **2017**, *17*, 7606–7612.
- (33) Enslin, D.; Stjerndahl, M.; Nyten, A.; Gustafsson, T.; Thomas, J. O. A comparative XPS surface study of $\text{Li}_2\text{FeSiO}_4/\text{C}$ cycled with LiTFSI- and LiPF₆-based electrolytes. *J. Mater. Chem.* **2009**, *19*, 82–88.
- (34) Smith, A. J.; Burns, J. C.; Dahn, J. R. A High Precision Study of the Coulombic Efficiency of Li-Ion Batteries. *Electrochem. Solid-State Lett.* **2010**, *13*, A177–A179.
- (35) Zeng, X.; Xu, G. L.; Li, Y.; Luo, X.; Maglia, F.; Bauer, C.; Lux, S. F.; Paschos, O.; Kim, S. J.; Lamp, P.; Lu, J.; Amine, K.; Chen, Z. Kinetic Study of Parasitic Reactions in Lithium-Ion Batteries: A Case Study on $\text{LiNi}_{0.6}\text{Mn}_{0.2}\text{Co}_{0.2}\text{O}_2$. *ACS Appl. Mater. Interfaces* **2016**, *8*, 3446–3451.
- (36) Shaju, K. M.; Rao, G. V. S.; Chowdari, B. V. R. Performance of layered $\text{LiNi}_{1/3}\text{Co}_{1/3}\text{Mn}_{1/3}\text{O}_2$ as cathode for Li-ion batteries. *Electrochim. Acta* **2002**, *47*, 145–151.

(37) Wu, Z.; Han, X.; Zheng, J.; Wei, Y.; Qiao, R.; Shen, F.; Dai, J.; Hu, L.; Xu, K.; Lin, Y.; Yang, W.; Pan, F. Depolarized and fully active cathode based on $\text{LiNi}_{0.5}\text{Co}_{0.2}\text{Mn}_{0.3}\text{O}_2$ embedded in carbon nanotube network for advanced batteries. *Nano Lett.* **2014**, *14*, 4700–4706.

(38) Wang, Z.; Sun, Y.; Chen, L.; Huang, X. Electrochemical Characterization of Positive Electrode Material $\text{LiNi}_{1/3}\text{Co}_{1/3}\text{Mn}_{1/3}\text{O}_2$ and Compatibility with Electrolyte for Lithium-Ion Batteries. *J. Electrochem. Soc.* **2004**, *151*, A914–A921.

(39) Reddy, M. V.; Rao, G. V. S.; Chowdari, B. V. R. Synthesis by molten salt and cathodic properties of $\text{LiNi}_{1/3}\text{Co}_{1/3}\text{Mn}_{1/3}\text{O}_2$. *J. Power Sources* **2006**, *159*, 263–267.

(40) Park, S. H.; Yoon, C. S.; Kang, S. G.; Kim, H. S.; Moon, S. I.; Sun, Y. K. Synthesis and structural characterization of layered $\text{LiNi}_{1/3}\text{Co}_{1/3}\text{Mn}_{1/3}\text{O}_2$ cathode materials by ultrasonic spray pyrolysis method. *Electrochim. Acta* **2004**, *49*, 557–563.

(41) Shaju, K. M.; Subba Rao, G. V.; Chowdari, B. V. R. Influence of Li-Ion Kinetics in the Cathodic Performance of Layered $\text{LiNi}_{1/3}\text{Co}_{1/3}\text{Mn}_{1/3}\text{O}_2$. *J. Electrochem. Soc.* **2004**, *151*, A1324–A1332.

(42) Yuan, L.-X.; Wang, Z.-H.; Zhang, W.-X.; Hu, X.-L.; Chen, J.-T.; Huang, Y.-H.; Goodenough, J. B. Development and challenges of LiFePO_4 cathode material for lithium-ion batteries. *Energy Environ. Sci.* **2011**, *4*, 269–284.

(43) Yu, Y.; Wang, J.; Zhang, P.; Zhao, J. A detailed thermal study of usual $\text{LiNi}_{0.5}\text{Co}_{0.2}\text{Mn}_{0.3}\text{O}_2$, LiMn_2O_4 and LiFePO_4 cathode materials for lithium ion batteries. *J. Energy Storage* **2017**, *12*, 37–44.

(44) Baba, Y.; Okada, S.; Yamaki, J.-i. Thermal stability of Li_xCoO_2 cathode for lithium ion battery. *Solid State Ionics* **2002**, *148*, 311–316.

(45) Wang, J.; Yu, Y.; Li, B.; Zhang, P.; Huang, J.; Wang, F.; Zhao, S.; Gan, C.; Zhao, J. Thermal Synergy Effect between $\text{LiNi}_{0.5}\text{Co}_{0.2}\text{Mn}_{0.3}\text{O}_2$ and LiMn_2O_4 Enhances the Safety of Blended Cathode for Lithium Ion Batteries. *ACS Appl. Mater. Interfaces* **2016**, *8*, 20147–20156.

(46) Zhang, L.; Ma, Y.; Cheng, X.; Zuo, P.; Cui, Y.; Guan, T.; Du, C.; Gao, Y.; Yin, G. Enhancement of high voltage cycling performance and thermal stability of $\text{LiNi}_{1/3}\text{Co}_{1/3}\text{Mn}_{1/3}\text{O}_2$ cathode by use of boron-based additives. *Solid State Ionics* **2014**, *263*, 146–151.